

PREDICTION OF AEROSOL HAZARDS ARISING FROM THE OPENING OF AN ANTHRAX-TAINTED LETTER IN AN OPEN OFFICE ENVIRONMENT USING COMPUTATIONAL FLUID DYNAMICS

FUE-SANG LIEN^{1,*}, HUA JI², EUGENE YEE³, BILL KOURNIKAKIS³

¹Department of Mechanical and Mechatronics Engineering, University of Waterloo,
Waterloo, ON, N2L 3G1, Canada

²Waterloo CFD Engineering Consulting Inc. 534 Paradise Crescent, Waterloo,
ON, N2T 2N7, Canada

³Defence R&D Canada – Suffield, P.O. Box 4000 STN MAIN, Medicine Hat,
AB, T1A 8K6, Canada

*Corresponding Author: fslien@uwaterloo.ca

Abstract

Early experimental work, conducted at Defence R&D Canada–Suffield, measured and characterized the personal and environmental contamination associated with simulated anthrax-tainted letters under a number of different scenarios in order to obtain a better understanding of the physical and biological processes for detecting, assessing, and formulating potential mitigation strategies for managing the risks associated with opening an anthrax-tainted letter. These experimental investigations have been extended in the present study to simulate numerically the contamination from the opening of anthrax-tainted letters in an open office environment using computational fluid dynamics (CFD). A quantity of 0.1 g of *Bacillus atrophaeus* (formerly referred to as *Bacillus subtilis var globigii* (BG)) spores in dry powder form, which was used here as a surrogate species for *Bacillus anthracis* (anthrax), was released from an opened letter in the experiment. The accuracy of the model for prediction of the spatial distribution of BG spores in the office from the opened letter is assessed qualitatively (and to the extent possible, quantitatively) by detailed comparison with measured BG concentrations obtained under a number of different scenarios, some involving people moving within the office. The observed discrepancy between the numerical predictions and experimental measurements of concentration was probably the result of a number of physical processes which were not accounted for in the numerical simulation. These include air flow leakage from cracks and crevices of the building shell; the dispersion of BG spores in the Heating, Ventilation, and Air Conditioning (HVAC) system; and, the effect of deposition and re-suspension of BG spores from various surfaces in the office environment.

Keywords: Anthrax-tainted letters, Computational fluid dynamics, Indoor dispersion, Open office environment.

Nomenclatures

C	Concentration, g/m ³
\bar{C}	Time-averaged concentration, g/m ³
c_m	Measured concentration value, g/m ³
k	Turbulence kinetic energy, m ² /s ²
T_{ON}	Tracer release period, s
t	Time, s

Greek Symbols

ε	Dissipation rate of turbulence kinetic energy, m ² /s ³
Δt	Time step, s

Subscripts

A, B, C	Sampler locations, Fig. 1
LO	Location of letter opener, Fig. 11
SKC	Location of SKC samplers, Fig. 11

Abbreviations

ACPLA	Agent containing particles per liter of air
BG	<i>Bacillus atropheus</i> (formerly known as <i>Bacillus subtilis var globigii</i>)
CBW	Chemical and biological warfare
CFD	Computational fluid dynamics
CFM	Cubic feet per minute
CFU	Colony forming unit
CW	Co-worker
DRDC	Defence R&D Canada
EIM	Eddy interaction model
GCIBM	Ghost-cell immersed boundary method
HR	High-resolution slit samplers
HVAC	Heating, ventilation, and air conditioning
IBM	Immersed boundary method
LO	Letter opener
LR	Low-resolution slit samplers
NIOSH	National institute for occupational safety and health
QUICK	Quadratic upstream interpolation for convective kinematics
RANS	Reynolds-averaged Navier-Stokes
SIMPLE	Semi-implicit method for pressure-linked equations
TVD	Total variation diminishing
UMIST	Upstream monotonic interpolation for scalar transport

1. Introduction

The incident involving anthrax-tainted letters sent in the autumn of 2001 to major media outlets and two United States senators [1], which resulted in five deaths and 17 non-fatal infections, has reinforced public concern on the threat of terrorist

use of chemical and biological warfare (CBW) agent weapons against civilian populations in dense urban centers. In previous experimental work [2-5], Defence R&D Canada–Suffield (DRDC–Suffield) measured and characterized the personal and environmental contamination associated with simulated anthrax-tainted letters under a number of different scenarios, in order to obtain a better understanding of the physical and biological processes for detecting, assessing, and formulating potential mitigation strategies for managing the risks associated with opening an anthrax-tainted letter. These experimental investigations in multiple small offices have been extended to characterize the contamination from anthrax-tainted letters in an open office environment. In a related study, Price et al. [6] investigated recently the risk to occupants in a building resulting from resuspension of deposited anthrax spores on indoor surfaces.

Practical mathematical models for prediction of dispersion of anthrax spores from opened letters in an indoor environment, which include the effects of people moving in the various offices on the dispersion, do not exist owing to the inherent complexity of the problem. There are an enormous number of possible scenarios for incidents involving anthrax-tainted letters due to their deliberate nature. Furthermore, the physical insight and concomitant data necessary to perform and validate the model predictions for most scenarios involving anthrax-tainted letters are (until recently) rather limited. In addition, the parameters required by the model (e.g., deposition velocity of anthrax spores on various types of surfaces) and the data needed to infer these parameters are not available. In spite of these complications, Reshetin and Regens [7] developed a box model to investigate the dispersion of anthrax spores released in a high-rise building. Following from this work, we will show in the present study that a more sophisticated modeling approach based on computational fluid dynamics (CFD) is able to make credible predictions of both the flow characteristics inside buildings (and, more specifically in an office within a building) and the concomitant dispersion of contaminants (e.g., anthrax spores from an opened letter) released into these flows.

The objective of the present study is to undertake a critical assessment of the utility of current CFD models for the prediction of flow and dispersion in the indoor environment. In particular, CFD modeling of the dispersion of a biological simulant *Bacillus atrophaeus* [formerly known as *Bacillus subtilis var globigii* (BG)] for anthrax, released from an opened letter in a large office (open office concept), will be undertaken. The accuracy of the model for prediction of the spatial distribution of BG spores in the office will be assessed qualitatively (and to the extent possible, quantitatively) by detailed comparison with measured BG spore concentrations obtained under a number of scenarios. In Section 2, the basic numerical framework for the CFD model used for these numerical studies, including the capability for simulating the movement of people in an office will be described. Section 3 will compare predictions against a baseline experiment in which a tracer gas (sulfur hexafluoride, or SF₆) was released in an open office in the west wing of Building 13 on the DRDC–Suffield campus. In Section 4, three scenarios involving the release of BG spores from an opened letter will be described, and various comparisons between model predictions and experimental measurements will be made for each scenario. Finally, conclusions drawn from the present study and recommendations made for future studies are given in Section 5.

2. Numerical Method

The STREAM code [8] was used in the present study for our numerical simulations. STREAM is a fully-conservative, block-structured finite-volume code for computational fluid dynamics, which employs a fully-collocated storage arrangement for all transported properties, including various turbulence quantities (e.g., turbulence kinetic energy, viscous dissipation rate, etc.). Within an arbitrary non-orthogonal coordinate system, the velocity vector is decomposed into its Cartesian components, and these are the components to which the momentum equations relate. Advective cell-face fluxes are approximated by the Upstream Monotonic Interpolation for Scalar Transport (UMIST) scheme [9], obtained by formally imposing Total Variation Diminishing (TVD) constraints on Leonard's third-order accurate Quadratic Upstream Interpolation for Convective Kinematics (QUICK) scheme [10]. A second-order fully implicit three-level scheme is used to treat the transient (or, local tendency) term. The mass continuity is enforced by solving a pressure-correction equation using the Semi-Implicit Method for Pressure-Linked Equations (SIMPLE) algorithm, which steers, as part of the iterative sequence, the pressure towards a state in which the mass residuals in all cells of the flow domain are negligibly small.

All transport equations, including mean momentum, turbulence and scalar concentration equations, are discretised and solved sequentially as part of the SIMPLE algorithm [11]. The linearized and discretised equations obtained in the outer iterations of the SIMPLE algorithm are solved numerically using very efficient iterative linear equation solvers, such as Stone's Strongly Implicit Procedure (SIP3D) [12] or the Conjugate Gradient Stabilized (CGSTAB) method. In conjunction with a fully-collocated approach, the SIMPLE algorithm is known to provoke checkerboard oscillations in the pressure field, reflecting a state of velocity-pressure decoupling. To avoid this, the widely used method of Rhie and Chow [13] has been adopted to interpolate the cell-face velocities from the adjacent nodal values. This interpolation essentially introduces a fourth-order "pressure smoothing" to remove the checkerboard oscillations in the pressure field. Physical diffusion fluxes are approximated using a conventional second-order accurate central differencing approach.

For mesh generation, the "ray-casting" approach [14] is used to determine whether a computational cell lies inside the complex geometry of objects encountered in the current problem, such as desks, partitions, and people in the study area. If the cell centroid is inside an object, the flag associated with this cell will be set to OBJECT. Otherwise, the cell flag is set to FLUID, allowing an efficient matrix solver (e.g., SIP3D) to be utilized for the solution of the discretised equations.

In order to numerically model one or more persons "entering or leaving" the office, we have investigated the use of the Immersed Boundary Method (IBM) [15] or its variants [16] to handle moving objects. The original IBM [15] represented a boundary of a solid body in the flow field through a forcing term (or a feedback function) that is added to the mean momentum equations. These forcing terms were evaluated initially at discrete points on the surface of the body, and were designed to enforce the no-slip boundary conditions on this surface. Subsequently, a first-order cosine function (which can be interpreted as a discrete

function) was used to interpolate and extrapolate information between the immersed boundary and the background grid. Unfortunately, the use of the cosine-function formulation smeared out the solution over a thin finite band centered on the boundary, which in general could have an adverse effect on the solution accuracy. Furthermore, IBM may induce spurious oscillations and, consequently, restricted severely the size of the computational time step, especially when an explicit time-integration method was used for the flow solver.

To overcome these difficulties, other IBM variants such as the ghost-cell immersed boundary method (GCIBM) [16], have been proposed. In contrast to IBM, GCIBM uses ghost cells within the solid objects as boundary conditions, without having to explicitly introduce a forcing term into the mean momentum equation. The ghost cells are reconstructed using either linear or quadratic interpolation of the property values at the neighbouring fluid nodes in the physical domain and at the boundary node. Although IBM has been widely used, most previous researchers have incorporated it into explicit flow solvers based on a fractional-step method, which as mentioned above severely limits the maximum allowable time step that could be used for the integration. Moreover, very little work has been undertaken to date, to combine IBM with a high-Reynolds-number Reynolds-averaged Navier-Stokes (RANS) solver for turbulent flow problems. In the present study, we have successfully incorporated the GCIBM into STREAM to give a fully implicit time-stepping scheme that utilizes a standard k - ϵ turbulence model, in conjunction with wall functions as boundary conditions at the solid surfaces (e.g., walls). This advancement in the application of GCIBM permitted the simulation of moving boundaries corresponding to mobile objects (e.g., people) within the flow domain.

3. Sulfur Hexafluoride (SF_6) Release Experiments

Five tracer gas experiments [17], involving the release of SF_6 , were conducted by personnel from the National Institute for Occupational Safety and Health (NIOSH). These experiments were undertaken in a simulated open office complex (see Fig. 1) set up in Building 13 on the DRDC-Suffield campus. Furthermore, NIOSH personnel also measured the flow rates of all the supply and return ducts [in cubic feet per minute (CFM)] in this study area. The latter information was used to specify the inflow/outflow boundary conditions for our CFD simulations. For comparisons with our numerical simulations, only data from “Experiment 1” will be used. In this experiment, 2.5 liters of pure SF_6 was released over a short period of several seconds from an airtight syringe at location F (letter-opener position) in Fig. 1. Measurements of the time history of the SF_6 concentration in parts per million by volume (ppm) were made at six locations (namely, at locations A, B, C, D, E, and G) as shown in Fig. 1.

Because the dispersion of SF_6 in the study area is strongly influenced by the flow motion, it is informative to examine the model predictions of the flow field first. The flow field in the study area (open office) was computed using a grid of $94 \times 70 \times 30$ nodes in the x -, y - and z -directions, respectively. This grid is exhibited in Fig. 2. Initially, it is assumed that the direction of airflow from the air supply ducts is in the vertical (or z -) direction as indicated by the “big” arrows in Fig. 3. To understand the flow field in the study area, let us consider a vertical y - z cross-section in Area I near location F, as illustrated by the sketch on the right-hand-

side of Fig. 3. We expect to see a clockwise vortex flow motion in a vertical y - z plane that contains the discharging jet from one of the air supply ducts flush-mounted on the floor. The implication of this figure is that the flow motion in a selected y - z plane that contains an air supply duct can be quite energetic, contrasting with the fact that the flow motion in the x -direction is actually rather weak. This can be seen clearly in Fig. 4, which exhibits stream traces near the front part of the study area. We should note that the average velocity from the supply and return ducts is about 1 m s^{-1} . The magnitude of the average velocity in the study area is about 0.05 m s^{-1} . The average velocity in the x -direction is approximately -0.002 m s^{-1} , which confirms the above-mentioned assertion of a weak flow motion in the x -direction.

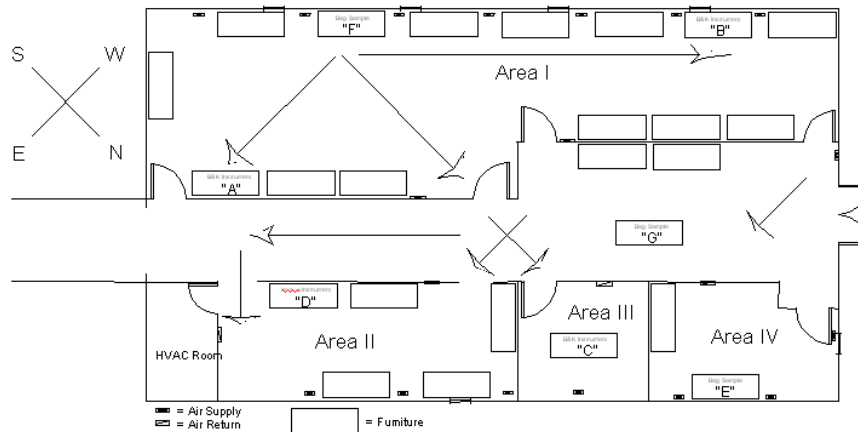


Fig. 1. Study Area in Building 13 Showing the Furniture Locations and the Positions of the Air Supply and Return Ducts. Furthermore, the Release Location (Location F) and Six Sampling Locations (Locations A, B, C, D, E, and G) for the Tracer Gas Used in the SF_6 Experiments are Shown.

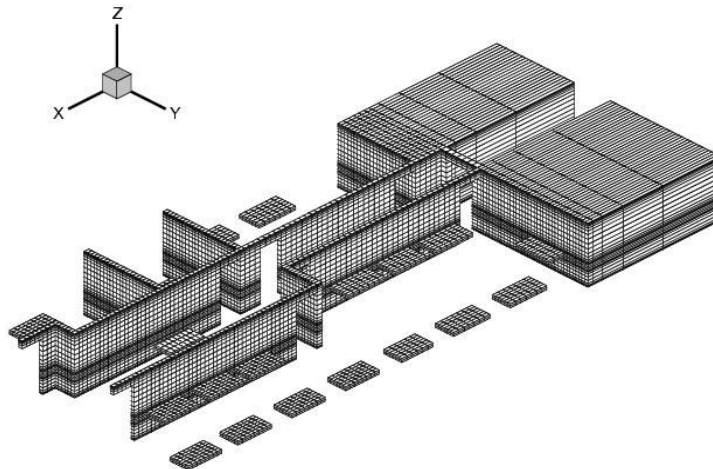


Fig. 2. Grid and Geometry used by CFD to Simulate the SF_6 Release Experiment in the Open Office Complex.

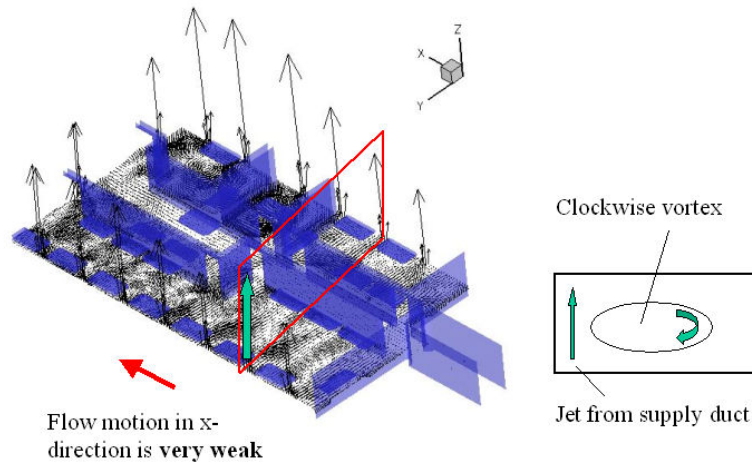


Fig. 3. Predicted Vortex Pattern in a Vertical y - z Plane for the SF_6 Experiment.

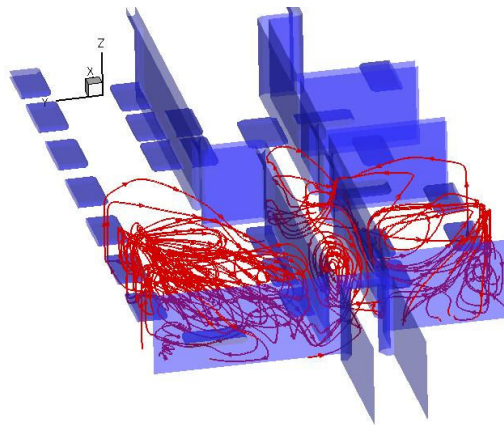


Fig. 4. Predicted Stream Traces in Area I near the Letter Opener (LO) for the SF_6 Experiment.

The release period for the SF_6 tracer is assumed to be $T_{\text{ON}} = 10$ s in the CFD simulation, although a release period of 5 s was also simulated with little observed effect on the final solution. In order to increase the time accuracy of the numerical prediction, the time step, t , for the simulation was chosen as follows: $\Delta t = 0.2$ s for $t \leq T_{\text{ON}}$; $\Delta t = 2$ s for $T_{\text{ON}} < t < 120$ s; and, $\Delta t = 10$ s for $t \geq 120$ s. The total time for the simulation is 7200 s after the initial release of the SF_6 tracer. The predicted time histories of the mean concentration of SF_6 at locations A, B, C, D, E, and G, along with comparisons to the corresponding experimental measurements, are shown in Fig. 5. At location A (collocated with co-worker 1), there is a sharp increase in the concentration-time profile in the experimental measurements, reaching a peak value of 20 ppm at $t = 180$ s (i.e., at 180 s after the

release of the SF₆ tracer). This peak concentration occurs much earlier than that predicted by the numerical simulation at the same location, where the predicted peak value of concentration is seen to be 10 ppm occurring at $t = 780$ s (13 min). Similarly, the experimental concentration measurements at location B (where co-worker 2 is collocated) achieves a peak concentration value of 11 ppm at $t = 300$ s (5 min). This needs to be compared with the predicted peak concentration value of 6 ppm at the time $t = 3000$ s (50 min) at this location. Again, the peak concentration value is under-predicted and occurs at a much later time.

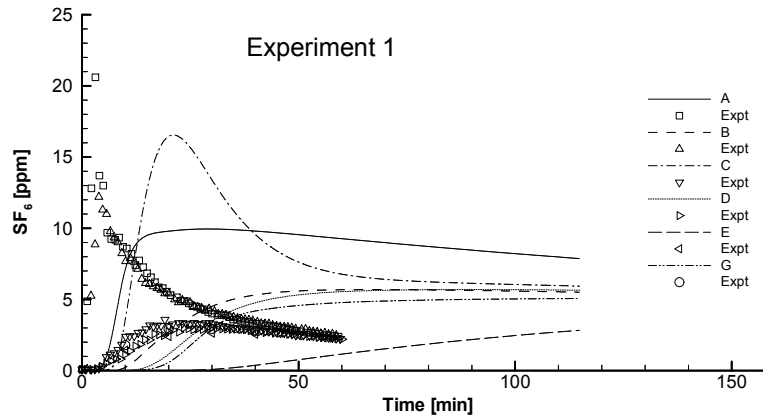


Fig. 5. Time Histories of Concentration in ppm from the CFD Predictions Compared with Experimental Measurements for the SF₆ Experiment.

In order to identify what might be the cause of the discrepancy in the predicted and observed cloud arrival times, two additional simulations were conducted. Firstly, a simulation was conducted for the same test problem using a finer mesh of $140 \times 100 \times 70$ nodes to investigate the effects of grid resolution on the fidelity of the prediction. It was found that this higher-resolution simulation gave essentially the same results as the original simulation, implying that grid resolution was not responsible for the discrepancy between the predicted and observed tracer concentration. Secondly, a simulation was conducted in which the direction of air flow at each supply duct location was deflected by grills at $\pm 45^\circ$ (in contrast to the original simulation in which the air flow from the supply duct was assumed to be in the vertical z -direction). Again, no major changes were observed in the predicted results.

In light of this, the discrepancy between the predicted and observed SF₆ concentration-time histories may be due to one or more of the following causes:

- In the actual situation, SF₆ released from location F can enter the return ducts (there are two return ducts in Area I) and, through the HVAC system re-enter the study area again through the supply ducts. However, this physical mechanism is not considered in the current CFD simulation. Although there are some 'zonal models', such as COMIS [18] and CONTAM [19], which are designed specifically for predicting dispersion of contaminants in the indoor environment with an inclusion of the effects of the HVAC system, these models are "one-dimensional

(1-D)” in the sense that they treat each room in a building as a well-mixed zone and, consequently, cannot be applied to the simulation of the complex 3-D flow and dispersion in a large office with furniture. The remedy for this problem is to develop a general procedure, which can couple the present CFD model (used to simulate the 3-D indoor flow and dispersion in the study area) with one of the zonal models (which can be used to simulate the flow and dispersion in the HVAC system, the latter of which is simply treated as a well-mixed zone).

- Building 13 on the DRDC–Suffield campus is an old vacated office building. The envelope or shell of this building is very leaky. Consequently, flow through cracks and crevices in the building envelope (e.g., window sills, walls, etc.), which have not been accounted for in our simulations, will undoubtedly generate additional air motions in the office. These air motions can significantly alter the dispersion of the SF₆ tracer in the office. To incorporate the effects of building leakage in our simulations, a “blower door” experiment will need to be conducted in order to identify the locations of the leakage points and to measure the flow rate through these points. With this additional information, it is conceivable that the predictive accuracy of our current CFD simulation results will be improved.

In addition to the two reasons enunciated above, anomalies in the experiment can also contribute to the observed discrepancy between the CFD predictions and the experimental measurements. To see this, let us also examine the results of Experiment 5 from the SF₆ release experiments [17], which are shown in Fig. 6. The major differences between Experiments 1 and 5 are as follows: in Experiment 1, pure SF₆ was released from an air-tight syringe for a release period of 30 s, whereas Experiment 5 involved the release of dilute SF₆ from a sampling pump for a release period of 60 s. Note that in Experiment 5, a dilute mixture consisting of one liter of pure SF₆ and 3 litres of air was used. Nevertheless, in spite of the differences in source strength in Experiments 1 and 5, the relative ratios of peak mean concentrations at locations A, B and D for each experiment should be the same (assuming that the nominal conditions in the office were unchanged between these experiments).

It is seen from Figs. 5 and 6 that $(C_A : C_B : C_D)_{\text{peak}} \approx (6.75 : 3.7 : 1)$ for Experiment 1 and $(C_A : C_B : C_D)_{\text{peak}} \approx (22.7 : 1.1 : 1)$ for Experiment 5, where C denotes the concentration and the subscript on C indicates the location where the concentration was measured. In our current simulation, $(C_A : C_B : C_D)_{\text{peak}} \approx (1.75 : 1 : 1)$. If we simply focus on $(C_B/C_D)_{\text{peak}}$, we find that $(C_B/C_D)_{\text{peak}} \approx 1.1$ from Experiment 5 is very close to our current prediction of $(C_B/C_D)_{\text{peak}} \approx 1$, which is encouraging. This seems to suggest that the much larger value of C_B (concentration at the co-worker 2 location) measured in Experiment 1 may be questionable, or at least not reproducible for the assumed nominal conditions existing in the office at the time of the measurements. It should be mentioned here that the very large peak value of concentration at location A (where co-worker 1 is located), in relation to the concentrations measured at the other sampler locations in Experiment 5, is probably also suspect. This assertion will be supported in Fig. 19 for Scenario 0 in the BG experiment (to be discussed later).

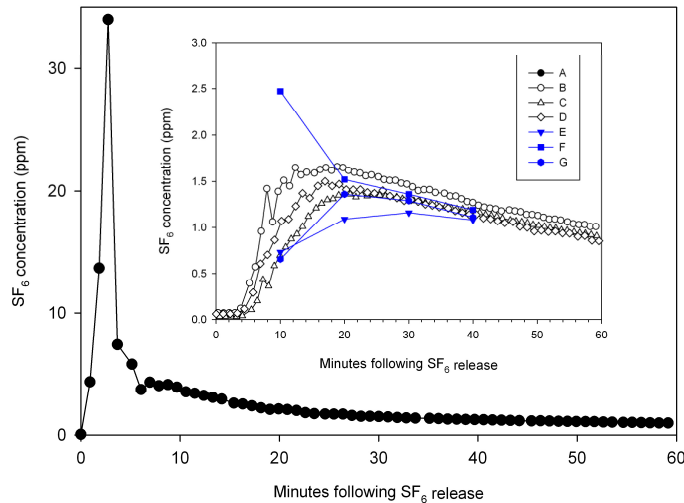


Fig. 6. Tracer Gas Experiment 5: Four Litres of a 1:3 Mixture of Pure SF₆ Tracer with Air is Released into the Room Using a Sampling Pump.

With reference to Fig. 6, the “well-mixed” condition for which concentration levels at all sampler locations are very similar, is clearly shown to be achieved (approximately or better) when $t = 3000$ s (50 min) in Experiment 1. However, even after 7200 s, the well-mixed condition was not achieved in our numerical simulation, particularly at locations A (co-worker 1) and E (sampler in Area IV), which is consistent with the iso-surfaces of concentration (ppm) at $t = 180$, 1200 and 7200 s (after the release) as shown in Figs. 7 to 9.

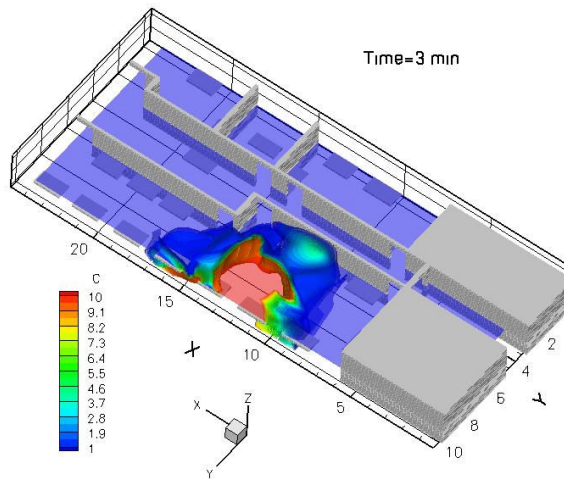


Fig. 7. Iso-Surfaces of Predicted Concentration in ppm from the CFD Predictions at $t = 3$ min for the SF₆ Experiment.

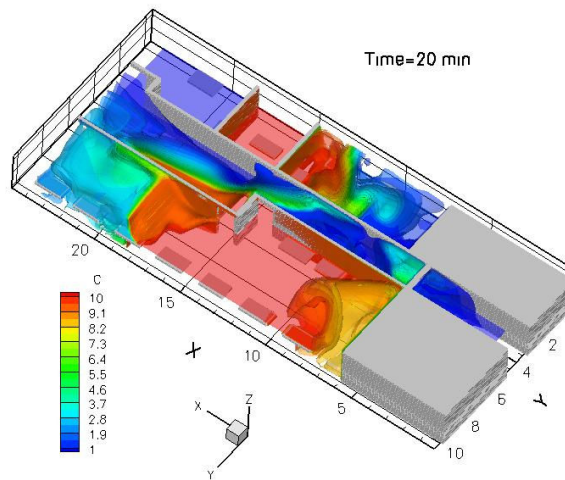


Fig. 8. Iso-Surfaces of Predicted Concentration in ppm from the CFD Predictions at $t = 20$ min for the SF_6 Experiment.

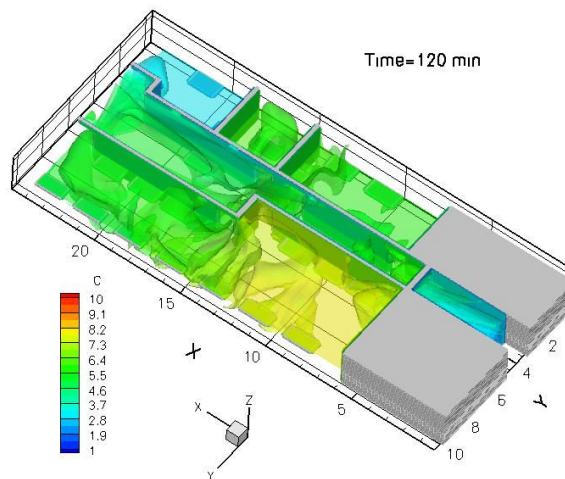


Fig. 9. Iso-Surfaces of Predicted Concentration in ppm from the CFD Predictions at $t = 120$ min for the SF_6 Experiment.

Finally, in order to demonstrate the capability of our CFD simulations in predicting accurately a transient release of a tracer in a “well-controlled” laboratory experiment, a prediction [20] of a mean concentration-time profile in the vertical center plane ($y = 0$) of an obstacle array at a height of $z/H = 0.25$ (H is the height of the obstacles) is shown in Fig. 10. As can be seen, an excellent agreement between predictions and measurements was achieved. Although agreement between the present CFD simulations and measurements for

Experiment 1 is less satisfactory, a result that is probably due to air flow leakage through the building envelope among other things, recommendations aimed at improving the present predictive results will be made in Section 5.

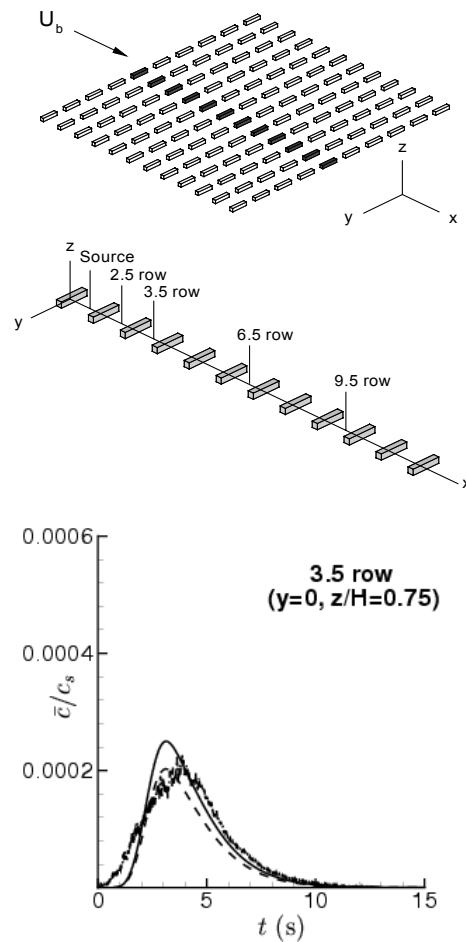


Fig. 10. Time History of the Predicted and Measured Normalized Mean Concentration Profile (Normalized by the Source Concentration) at the Vertical Center Plane ($y = 0$) of an Obstacle Array and at a Height $z/H = 0.75$. Solid and Dashed Lines: Predictions; Dash-dot Line: Experiment [20].

4. *Bacillus Atropheus* (BG) Release Experiments

Dispersion experiments, involving the release of BG spores in powder form from an opened letter, were conducted. These experiments simulated a number of different scenarios. Three of these scenarios, described in Sections 4.1 to 4.3, were simulated using CFD.

4.1. Scenario 0 (Baseline Case)

A source of 0.1 g of BG spores in powder form was placed in a sealed envelope. This envelope was located at the position occupied by the LO (Letter Opener), as shown in Fig. 11. To simplify the notation henceforth, Co-worker 1 and Co-worker 2 in Fig. 11 will be referred to as CW1 and CW2, respectively. The LO (person) was positioned about 0.5 m in front of the source location (sealed envelope containing the BG spores). The office geometry and grid, consisting of $116 \times 74 \times 30$ nodes in the x -, y - and z -directions, respectively, are shown in Fig. 12. Note that the major differences between Figs. 2 and 12 are that partitions were added between the various desks in the study area, and the two middle doors in Area I (Fig. 12) were closed. The HVAC system was turned on for about 15 min until the flow reaches a pseudo-steady state condition before the sampling process began. The sampling process lasted for 30 min. During the sampling stage, the HVAC was still on, and the front and rear doors in Area I were open. As for the SF_6 experiment described earlier, BG spores entering the return ducts were assumed to be released directly to the outdoor environment (viz., no spores entering the return ducts were allowed to re-enter the study area through the supply ducts) in the present simulations. The (unknown) effects of deposition and re-suspension of BG spores in the study area were not considered here (viz., walls and other surfaces in the open office were assumed to be perfect reflectors in the sense that no BG spores were deposited on these surfaces). Immediately after the BG spores were released (viz., after the letter was opened), the LO remained stationary for the remainder of the test period. The total release time for the BG spores was assumed to be 10 s.

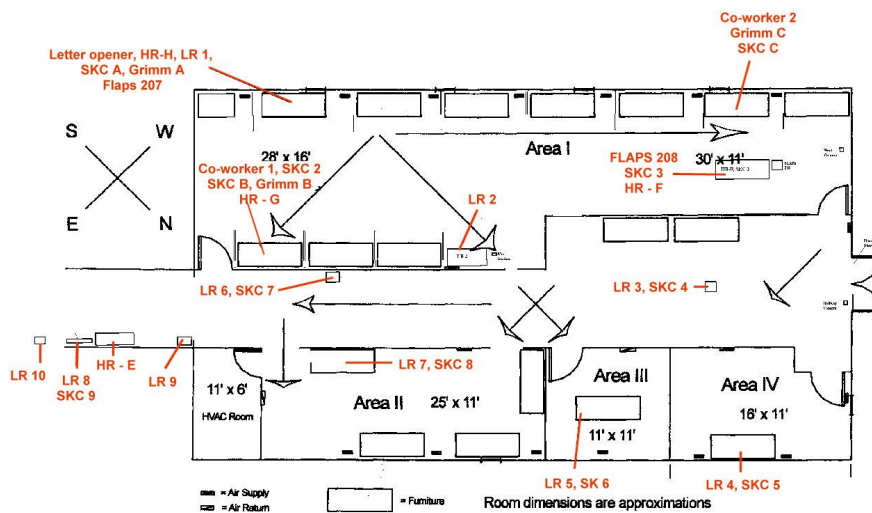


Fig. 11. Study Area in Building 13 Showing Furniture Layout, Locations of Air Supply and Return ducts, and Release and Sampling Locations for the BG Release Experiments.

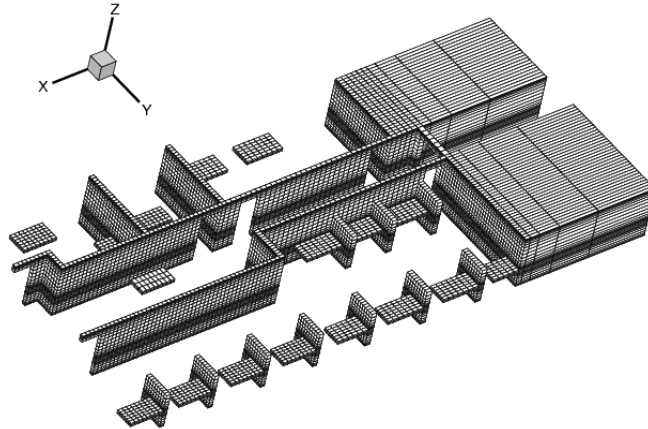


Fig. 12. Grid and Geometry Used by CFD to Simulate the BG Release Experiments.

Contours of $\log_{10}(100C)$, where C is the concentration in g/m^3 , are shown in Fig. 13 at $t = 8.75$ s and in Fig. 14 at $t = 1800$ s (30 min). Note that the presence of the LO in Fig. 14 obstructs the spread of the BG spores. Concentration contours in Fig. 14 suggest that BG spores have already dispersed into the entire study area at $t = 1800$ s (30 min), with concentrations in regions in or close to Area IV being the smallest. The unit for the predicted concentration “ C ” shown in Figs. 15, 16 and 18 is g/m^3 . This is different than the unit of measured concentration used in Fig. 19 (namely, Agent Containing Particles Per Liter of Air (ACPLA) used for the measurements made by the slit samplers) and in Fig. 17 [namely, Colony Forming Unit (CFU) per Liter of Air used by the SKC samplers]. Since the exact conversion between g/m^3 , ACPLA and CFU per Liter of Air is unknown, the comparisons between our CFD predictions and the experimental measurements need to be interpreted with care. In performing the analysis of the filters from the SKC samplers, the data from the slit samplers were used to determine the cloud arrival time at each location. In our simulations, the cloud arrival time at each location is estimated from the concentration-time history at each of the SKC locations. For example, by reference to Fig. 15, the arrival time $T_{\text{start}} = 273$ s at location SKC-2. This was used as the start time to compute the time-averaged concentration using the following formula

$$\bar{C} = \frac{1}{T_{\text{end}} - T_{\text{start}}} \int_{T_{\text{start}}}^{T_{\text{end}}} C dt \quad (1)$$

where the end time, T_{end} , is set to be 1800 s (30 min).

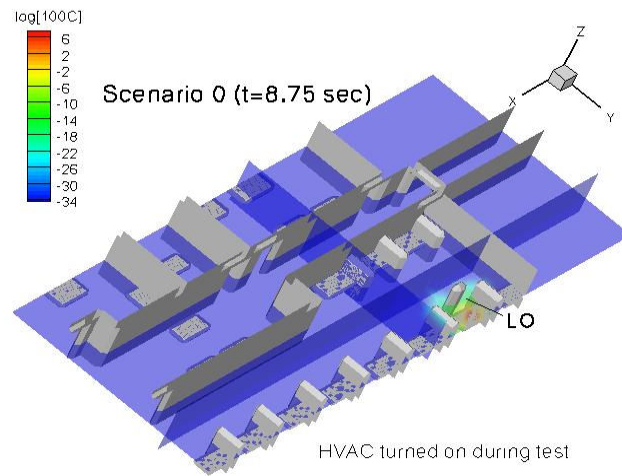


Fig. 13. Contours of Predicted Concentration for Scenario 0 (Baseline Case) at $t = 8.75$ s.

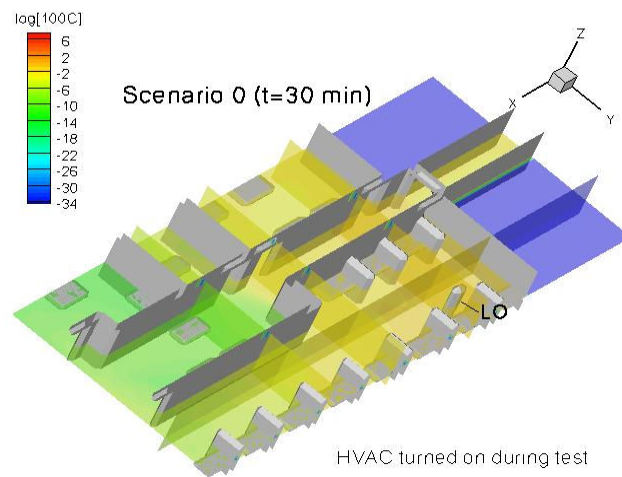


Fig. 14. Contours of Predicted Concentration for Scenario 0 (Baseline Case) at $t = 1800$ s (30 min).

Bar plots of predicted concentration in g/m^3 at 9 different SKC sampler locations (summarized in Fig. 11) are exhibited in Fig. 16. This figure should be examined in conjunction with Fig. 17, for which the concentration unit is expressed

as CFU per Liter of Air. Note from Fig. 16 that the SKC-1 and LO samplers are located close to each other; namely, the SKC-1 sampler was placed on the desk in front of which the letter opener was seated, whereas the LO sampler was worn by the letter opener. Both of these samplers were located in the vicinity of the center of the desk where the sealed envelope, containing the BG spores, was placed. Not surprisingly, the concentrations at SKC-1 and LO in Fig. 17 are different, with the concentration at LO being the largest in the experiment (Trial 3). It is seen from Fig. 17 that the concentration level at SKC-2 (or CW1) is the second largest due to its proximity to LO. The concentration levels at SKC-7 (in the hallway), SKC-8 (in Area II) and SKC-9 (in the exit area) are of the same order of magnitude, all of which are smaller than that at SKC-2. However, concentrations at the above-mentioned three locations are reduced drastically for Scenario 1 (see Figs. 22 and 24), in which the front door in Area I is closed after $t = 5.5$ s.

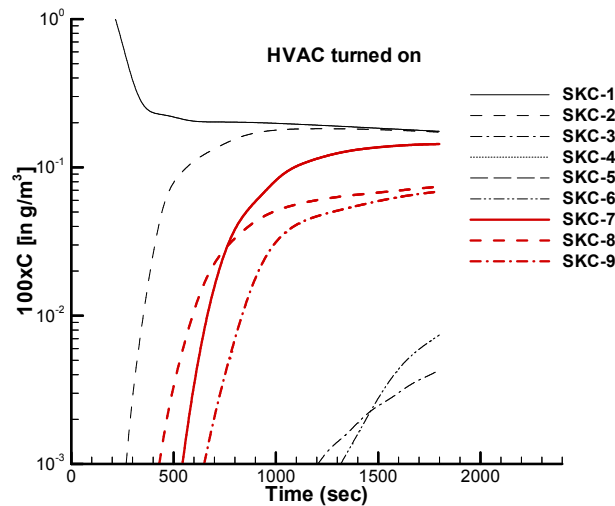


Fig. 15. Time Histories of Predicted Concentration at the SKC Sampler Locations for Scenario 0 (Baseline Case).

Concentrations at SKC-3 to SKC-6 shown in Figs. 16 and 17 are significantly smaller than those at the other locations, owing to their greater separation from the LO. The concentration level at the LO is $O(10^2)$ larger than that at SKC-2 in the experiment, which differs markedly from the current simulation which shows that $[C_{LO}/C_{SKC-2} \approx O(10^3)]$. Here $O(10^n)$ means 'of the order of magnitude of 10^n ', where n is an integer exponent. In contrast, concentration levels at SKC-7 to SKC-9 from the experiment are quite similar, which agrees well with our numerical predictions (cf. Fig. 16). Another major difference shown in Figs. 16 and 17 is that concentration levels at SKC-3 to SKC-6 in the experiment are not insignificant compared to those at SKC-7 to SKC-9. This might be due to (1) air leakage through cracks and crevices in the building envelope, and (2) BG spores

re-entering the study area through the HVAC system. Both effects are not accounted for in the simulations.

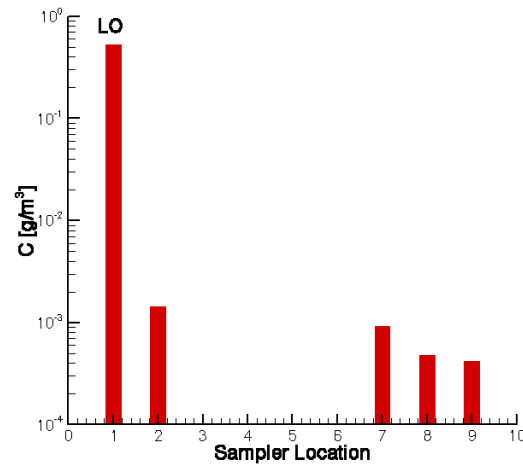


Fig. 16. Bar Charts of Predicted Concentration in g/m^3 at the SKC Sampler Locations for Scenario 0 (Baseline Case).

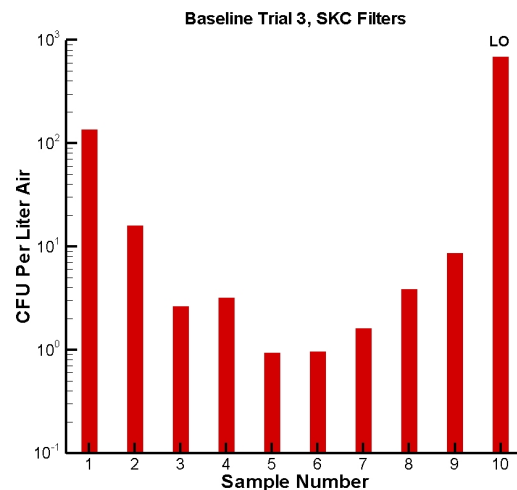


Fig. 17. Bar Charts of Measured Concentration from Experiment (Trial 3) in CFU per Liter of Air at the SKC Sampler Locations for Scenario 0 (Baseline Case).

The time histories of concentration at the locations of the high-resolution (HR) slit sampler in g/m^3 (present calculations) and in ACPLA (experimental measurements) are shown in Figs. 18 and 19, respectively. It can be seen from

Fig. 18 that the predicted concentration at the LO is much larger than that at CW1, which attains the second largest concentration shown in the figure. In contrast, from Fig. 19, it can be seen that the concentration at HR-H (or LO in Fig. 18) is only about two times larger than that at HR-G (or CW1 in Fig. 18). As mentioned before, the conversion between g/m^3 and ACPLA is not known, owing to the fact that the number of spores in each colony forming unit (CFU) is not known. Therefore, it is difficult to make an unambiguous comparison between the numerical predictions and the experimental measurements. Nevertheless, to ensure that global mass conservation in the present simulation is satisfied, the total mass released from the source (at the LO position) for $t \geq 10$ s is calculated by integrating the concentration over the volume of the entire study area, which we found to be equal to 0.102 g. This value is essentially identical to the total mass of 0.1 g released from the source¹. After checking the global mass conservation in our calculations, we postulated that the above-mentioned discrepancy could be caused by

- only one control volume with a length scale of about 8.7 cm was used in the present simulation to represent the source (i.e., the letter containing the BG spores);
- the release period of 10 s was arbitrarily assumed;
- deposition and re-suspension of BG spores were not accounted for in the simulation;
- the opening of the letter resulted in the release of all 0.1 g of BG spores (although in reality only a small fraction of the total mass of BG spores in the opened letter was released).

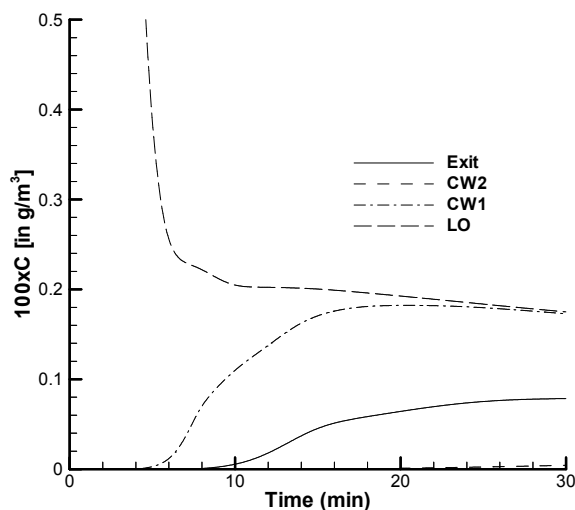


Fig. 18. Time Histories of Predicted Concentration in g/m^3 at the Locations of the High-Resolution Slit Samplers (HR) for Scenario 0 (Baseline Case).

¹ Although in our simulations, we assumed that the total mass of 0.1 g of material in the envelope was released after it was opened, in actuality, the mass of material released was much smaller (probably about 2–3 percent of the total 0.1 g of material in the envelope was actually released).

Qualitatively speaking, the general trends observed at CW1 (or HR-G), CW2 (or HR-F) and Exit (or HR-E) in Figs. 18 and 19 were similar. The concentration level at CW2 is the smallest among the four HR locations examined. This is because (1) the separation between LO and CW2 is the largest, and (2) the flow velocity in the x - (or LO-to-CW2) direction is very small ($\approx -0.002 \text{ m s}^{-1}$) as shown in earlier in Fig. 3. Furthermore, it can be seen from Figs. 18 and 19 that the concentration level at Exit is the second smallest for this scenario because (1) the separation between LO and Exit is smaller than that between LO and CW2, and (2) the front door in Area I is open during the test.

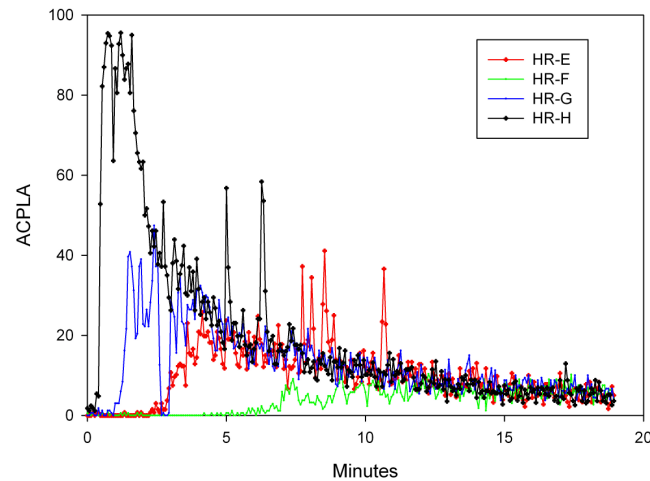


Fig. 19. Time Histories of Measured Concentration in ACPLA from Experiment (Trial 3) at the Locations of the High-Resolution Slit Samplers (HR) for Scenario 0 (Baseline Case).

4.2. Scenario 1

For this scenario, two additional personnel (CW1 and CW2) were involved. A source of 0.1 g of BG spores in powder form was placed in a sealed envelope and positioned at the location of the “Letter Opener” (LO) shown in Fig. 11. The experimental personnel (LO, CW1 and CW2) were positioned initially about 0.5 m in front of the tables (marked by Letter Opener, Co-worker 1 and Co-worker 2 in Fig. 11). The HVAC system was turned on for about 15 minutes until the flow reached a pseudo-steady state condition in the office, after which the BG spores were released by opening the sealed envelope. The latter process was assumed to take 10 s. Immediately after the BG spores were released from the opened envelope, LO, CW1 and CW2 began to walk along the footprint pathway (trail) laid out on the floor of the study area (shown in Fig. 20), finally exiting through the exit door. The speed of walking of each person was about 1 ms^{-1} . It took approximately 12, 11 and 28 s for LO, CW1 and CW2 to walk through the study area and exit through the exit door, respectively. The HVAC system was shut down when CW1 passed the

HVAC room (at $t = 5.5$ s). The front door in Area I (close to the Co-worker 1 location in Fig. 11) was closed after the LO passed through it.

The rear door in Area I was left open during the simulation, in order to satisfy “global mass conservation” in the study area (Areas I to IV plus the hallway). Although the flow rates in cubic feet per minute (CFM) from all supply and return ducts are provided by the experimental measurements and adjusted slightly to satisfy

$$\sum \text{CFM}_{\text{supply ducts in study area}} \neq \sum \text{CFM}_{\text{return ducts in study area}} \quad (2)$$

mass conservation was not necessarily satisfied in Area I alone from the measurements; i.e.

$$\sum \text{CFM}_{\text{supply ducts in Area I}} \neq \sum \text{CFM}_{\text{return ducts in Area I}} \quad (3)$$

Equation (3) corresponds to the condition that prevailed when both front and rear doors in Area I were closed. This caused numerical convergence problems in our simulation. For this reason, the rear door was left opened throughout the entire time period (30 minutes) for our simulation. This is the same time interval for which the low-resolution (LR) slit samplers was activated in the experiment.

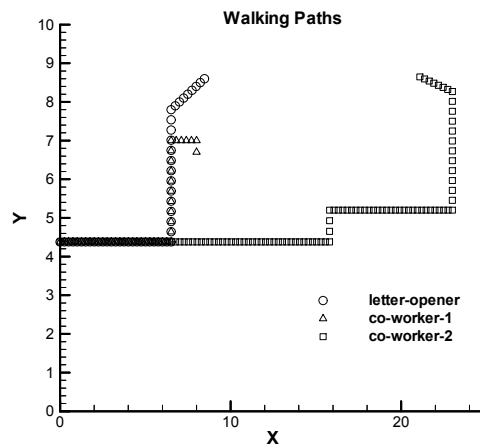


Fig. 20. The Walking Paths Used by LO, CW1 and CW2 to Exit the Study Area for Scenarios 1 and 2.

Two cases were considered for Scenario 1. In Scenario 1a, the HVAC system was turned on throughout the entire simulation period. In Scenario 1b, the HVAC system was shut down by CW1 at time $t = 5.5$ s. Note that Scenario 1a is performed here as an interesting complement (since no experimental data is available for this case) to Scenario 1b, in order to investigate the effect of the HVAC system on the dispersion of the BG spores from the opened envelope. At $t = 8.75$ s, the BG concentration contours for these two scenarios are very similar (not shown). This is because the HVAC system has just been turned off at $t = 5.5$ s for Scenario 1b. At $t = 1800$ s (30 min), however, Fig. 21 shows that the dispersion of BG spores in the study area is significant for the scenario in which the HVAC system was left on for the entire simulation time. The cloud in this case is seen to disperse throughout Area I, and then spread through the rear door

to contaminate Areas IV, III and II through the doors in the hallway. In contrast, as clearly seen in Fig. 23, the dispersion of the BG spores in the open office at $t = 1800$ s (after the release) is still limited primarily to Area I when the HVAC system was shut down soon after the opening of the sealed envelope. This suggests that the advective mechanism, associated with a directed flow motion, is more important than the turbulent diffusive mechanism for the dispersion of BG spores for the current indoor conditions. Note that shutting down the HVAC system not only reduced the mean flow, but also the level of turbulence in the open office. Since the turbulent diffusion coefficient $\Gamma \propto k^2 / \varepsilon$ (k is the turbulence kinetic energy and ε is the dissipation rate of turbulence kinetic energy) is closely linked to the level of turbulence kinetic energy, shutting down the HVAC system can be a very effective means for reducing the dispersion of BG spores in the office, owing to the fact that both the advective and diffusive mechanisms for dispersion are suppressed simultaneously.

If the HVAC system is turned on as in Scenario 1a, it is very important to close both the front and rear doors to prevent the spread of BG spores from Area I to the other areas in the open office, including the hallway. It is interesting to compare Figs. 21 and 14 (Scenario 0) in order to see the effect of closing the front door in Area I on the dispersion of BG spores. As expected, when the front door is closed, the concentration contours in Fig. 21 show that the BG spores do not even disperse to the end of the exit area after $t = 1800$ s (30 min). Although we were unable to simulate a scenario where both doors in Area I were closed due to the fact that flow rates for both return and supply ducts were only measured when both doors were opened, it is expected that most BG spores from the opened letter will be “trapped” (and hence confined) inside Area I. Note that BG spores can also enter the return ducts in Area I and, through the HVAC system (if it is turned on) re-enter the hallway and Areas II to IV through the supply ducts. However, this mechanism was not considered in the present numerical study.

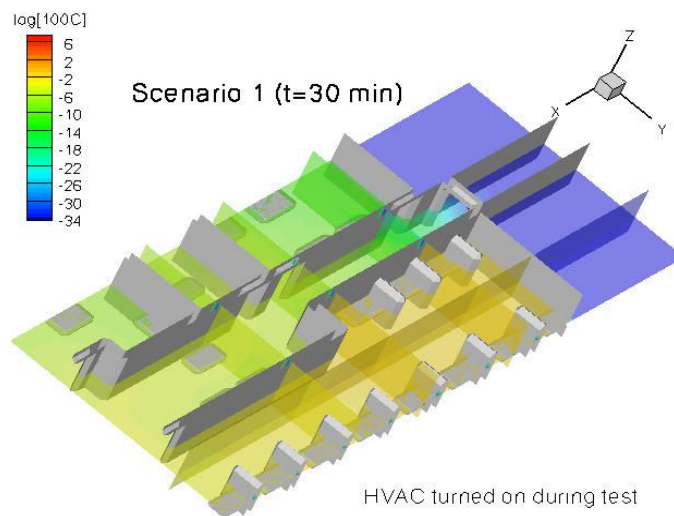


Fig. 21. Contours of Predicted Concentration for Scenario 1a (HVAC Turned on for the Entire Simulation Time) at $t = 1800$ s (30 min).

The bar plots of predicted concentration for Scenarios 1a and 1b are shown in Figs. 22 and 24, respectively, which should be examined in conjunction with Figs. 21 and 23. With the HVAC system turned on all the time (see Fig. 22), the concentration levels at SKC-2 to SKC-4 are larger than those with the HVAC system turned off after $t = 5.5$ s (see Fig. 24). In fact, the concentration levels at SKC-3 to SKC-9 in Fig. 24 are less than 10^{-4} g/m³. Fig. 24 can only be compared qualitatively with Fig. 25 (Trial 3 experiment) because the units of concentration are different (g/m³ compared to CFU per Liter of Air). As in Fig. 17, SKC-1 (sampler on desk) and LO (or SKC-A) sampler (worn by the letter opener) in Fig. 25 correspond to two different samplers that are at slightly different locations in the vicinity of the desk (as shown in Fig. 11). However, in our simulations, owing to the numerical resolution, the SKC-1 and LO samplers in Fig. 24 (simulation) represent exactly the same location, both of which are taken at the center of the desk (table). One encouraging result here is that $C_{LO}/C_{SKC-2} \approx O(10^3)$ for both the experimental measurements and the numerical simulation. It can be seen from Fig. 25 that the concentration levels at SKC-2 and SKC-3 are comparable, which contradicts the numerical predictions shown in Fig. 24 (where the concentration level at SKC-3 is seen to be much smaller than that at SKC-2). Since the HVAC system is turned off most of time in the experiment and in the Scenario 1b simulation, it is quite unlikely that the concentration level at SKC-2 (which is nearby LO) can be comparable to that at SKC-3. There are two reasons that could cause this “anomaly”: namely, (1) as LO passes close to SKC-3, it may have contaminated this sampler, leading to an increase in the observed concentration; or, (2) the air flow leakage through the building shell may be a cause for the above-mentioned difference.

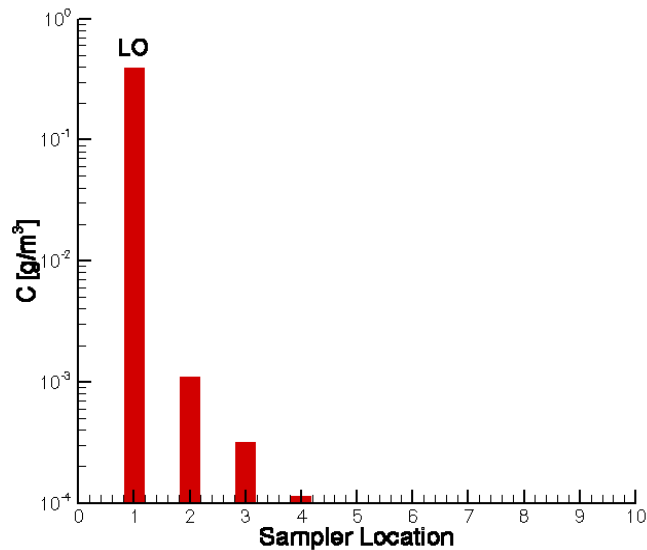


Fig. 22. Bar Charts of Predicted Concentration in g/m³ at the SKC Sampler Locations for Scenario 1a (HVAC Turned on for the Entire Simulation Time).

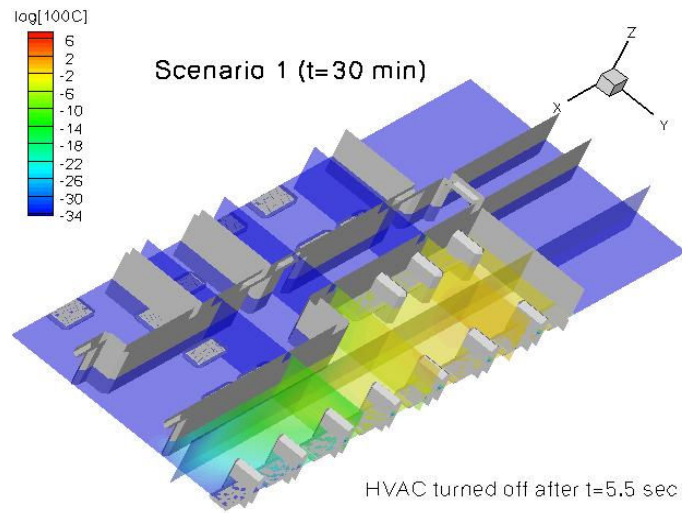


Fig. 23. Contours of Predicted Concentration for Scenario 1b (HVAc Turned off after $t = 5.5$ s) at $t = 1800$ s (30 min).

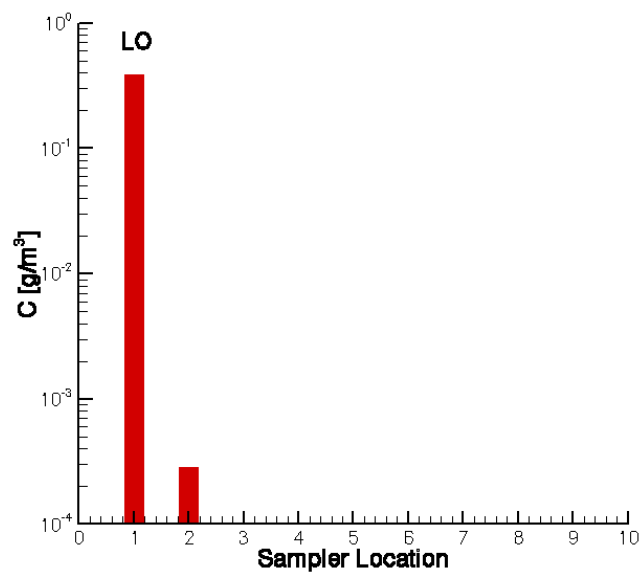


Fig. 24. Bar Charts of Predicted Concentration in g/m^3 at the SKC Sampler Locations for Scenario 1b (HVAc Turned off after $t = 5.5$ s).

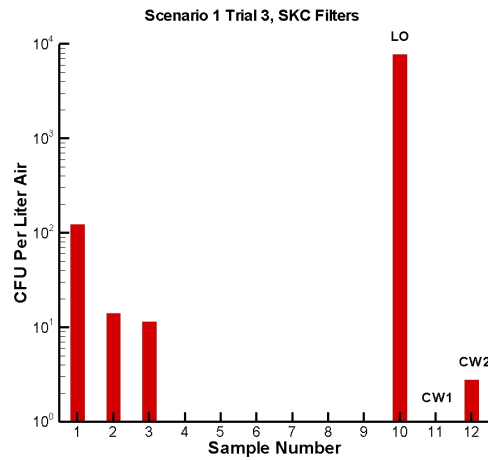


Fig. 25. Bar Charts of Measured Concentration from Experiment (Trial 3) in CFU per Liter of Air at the SKC Sampler Locations for Scenario 1.

4.3. Scenario 2

In Scenario 2, CW1 and CW2 leave Area I and exit through the exit door immediately after the BG spores were released from the opened letter. The LO remains still for 5 min before he too exits the test area, following the same footprint pathway as shown in Fig. 20. We only have flow rate measurements for the supply and return ducts when all the doors in Area I were opened as in the SF₆ experiment. However, we found that numerical convergence problems occurred in our simulations if all doors were closed, as mentioned earlier in the discussion following Eq. (3). Consequently, in the current simulation, the front door was closed only after the LO left the test area. The rear door of Area I was left opened throughout the test.

Figures 26 to 28 show contours of predicted concentration at $t = 8.75$ s (BG spores were still being released, while the LO remains stationary after opening the envelope), at $t = 310.75$ s (the LO is about to exit through the exit area), and at $t = 1800$ s (30 min). Since CW1 and CW2 leave the test area at a walking speed of about 1 m s^{-1} , which is much faster than the rate at which BG spores are dispersing near the LO, their motions practically cause no disturbance to the dispersion of BG spores. In this simulation, both doors in Area I remained open for the first 300 s. As a result, it is seen from Fig. 27 ($t > 300$ s) that the BG spores have already dispersed into the hallway near the exit area after the front door was closed. At the end of the simulation ($t = 1800$ s) shown in Fig. 28, a portion of the BG spores which were excluded from Area I in Fig. 27, have already spread in both directions from near the front door towards the exit area (to the right) and towards Areas II and III (to the left). Area IV is the only area for which the BG spores have not as yet dispersed into.

The BG spores have already dispersed into most parts of the study area (see Fig. 28 which shows the concentration contours on a logarithmic-scale) by $t = 1800$ s (30 min). Note that the predicted concentration levels at the SKC sampler locations, as seen in the bar plots of Fig. 29, show that at most of the sampler locations (SKC-3 to

SKC-9) the concentration was below 10^{-4} g/m^3 , with the exception of the locations at SKC-1 (or LO) and SKC-2 (or CW1). It is informative to compare Fig. 24 (in which the front door was closed after $t = 5.5 \text{ s}$) and Fig. 29 (in which the front door was closed after $t = 305.5 \text{ s}$). For both cases, the HVAC system was turned off after $t = 5.5 \text{ s}$. The concentration levels at LO and SKC-2 in both figures are very comparable, although concentration at SKC-2 in Fig. 24 is slightly smaller than that in Fig. 29. This might be due to the presence of the LO at the desk (during the first 5 min after the letter was opened) who may have obstructed (or, constrained) the spread of BG spores in the case of Fig. 29 (cf. Fig. 26).

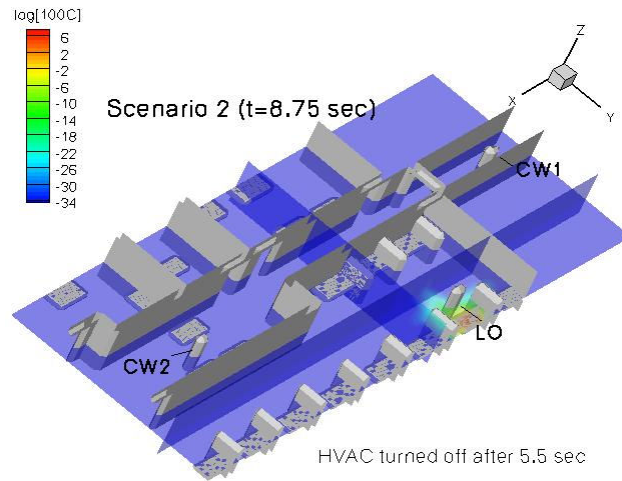


Fig. 26. Contours of Predicted Concentration for Scenario 2 at $t = 8.75 \text{ s}$ after the Opening of the Letter.

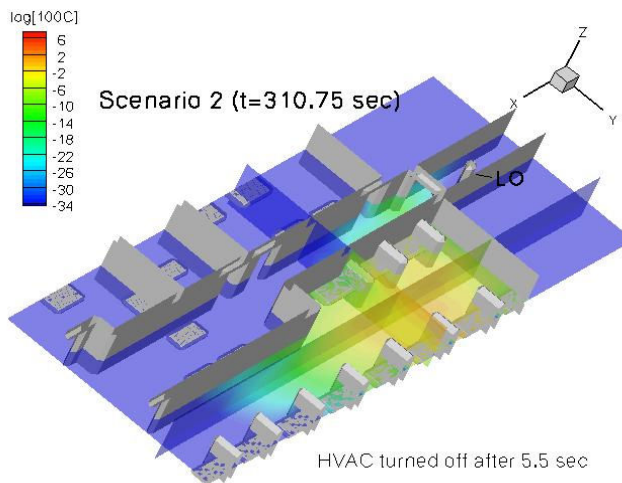


Fig. 27. Contours of Predicted Concentration for Scenario 2 at $t = 310.75 \text{ s}$ after the Opening of the Letter.

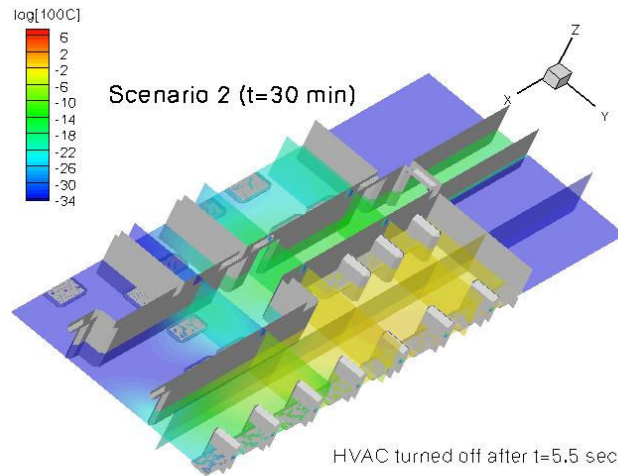


Fig. 28. Contours of Predicted Concentration for Scenario 2 at $t = 1800$ s (30 min) after the Opening of the Letter.

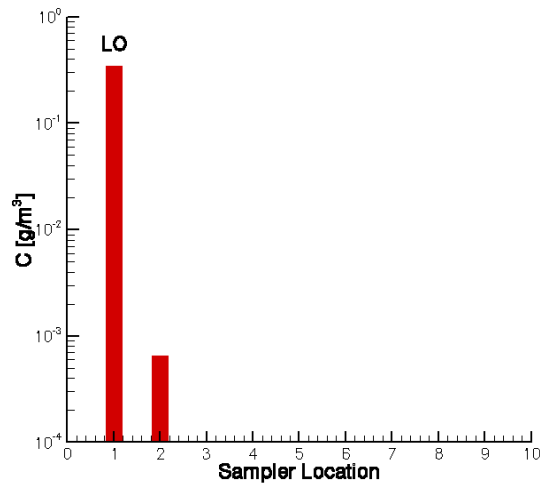


Fig. 29. Bar Charts of Predicted Concentration in g/m^3 at the SKC Sampler Locations for Scenario 2.

The experimental data (Trial 3) for this scenario, shown in Fig. 30 in CFU per Liter of Air instead of in g/m^3 , is quite different from the numerical predictions, especially in terms of C_{LO}/C_{SKC-2} . The predicted C_{LO}/C_{SKC-2} is $O(10^3)$, whereas the C_{LO}/C_{SKC-2} from the experimental measurements is $O(10)$. It should be noted here that $C_{LO}/C_{SKC-2} \approx O(10^3)$ in Scenario 1 for both the numerical predictions and the experimental measurements. The major difference between Figs. 25 and 30 is that the concentration levels at the SKC-2 and SKC-3 locations in the present scenario

(see Fig. 30) are $O(10)$ larger than those shown in Fig. 25 (Scenario 1). Also, the concentration level at the LO shown in Fig. 30 is $O(10)$ smaller than that shown in Fig. 25. Since the HVAC system was turned off in both experiments, it is possible that this discrepancy can be attributed to the air flow leakage through the cracks and crevices in the building shell, particularly in Scenario 2. Another contributing factor to the discrepancy might be an experimental anomaly. This is illustrated in Fig. 31, in which $C_{LO}/C_{SKC-2} \approx O(10^2)$ for Trial 5 and $C_{LO}/C_{SKC-2} \approx O(10)$ for Trial 3 (essentially an “identical” replication) as seen in Fig. 30, suggesting that the variability in measurements even on nominally identical replications is large.

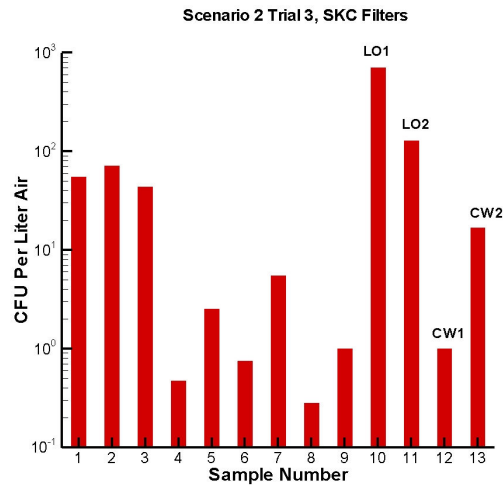


Fig. 30. Bar Charts of Measured Concentration from Experiment (Trial 3) in CFU per Liter of Air at the SKC Sampler Locations for Scenario 2.

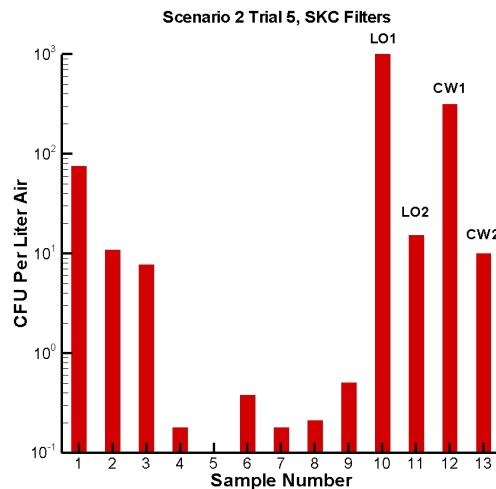


Fig. 31. Bar Charts of Measured Concentration from Experiment (Trial 5) in CFU per Liter of Air at SKC Sampler Locations for Scenario 2.

In this experiment, CW1 and CW2 exit the study area immediately after the LO informs them that he has opened a letter containing the BG spores. Both front and rear doors are closed as soon as CW1 and CW2 leave Area I. However, it is still possible that a small portion of BG spores deposit on CW1 and disperse into the study area outside Area I as CW1 walks along the prescribed path shown in Fig. 20. This hypothesis is supported by the reasonably high concentration levels measured at locations of SKC-4 to SKC-9, which are outside Area I. In contrast, the predicted concentration levels shown in Fig. 29 are less than 10^{-4} g/m³ at SKC-4 to SKC-9, because deposition and re-suspension are not considered in the numerical simulation.

5. Conclusions and Recommendations

In the present study, two experiments, namely SF₆ and BG spore release experiments were simulated using CFD. In the SF₆ release experiment, ventilation measurements in terms of volumetric flow rate were conducted, and the time histories of concentration in ppm at 6 sampler locations were available. This, in principle, could be predicted by CFD simulations if the laboratory environment (study area) is well controlled (viz., if there are no air flow leakages in the study area). The BG release experiments, however, were much more challenging to simulate because the concentration units used in the experimental measurements (e.g., CFU per Liter of Air or ACPLA) cannot be related unambiguously to the mass of BG spores released from the opened letter. More specifically, the number of spores in the sealed envelope in colony forming units (CFU) was unknown, and the actual number of BG spores released when the letter was opened was also unknown. Furthermore, the effect of deposition and re-suspension of BG spores in the indoor environment was not considered in our simulations. Therefore, we can only make qualitative, rather than quantitative comparisons, between the numerical predictions and the experimental measurements of BG concentration because the exact conversion between CFU per Liter of Air, ACPLA and g/m³ is not known. As well, the precise amount of BG spores released from the opened letter was not known.

In the case of the BG release experiments, three different scenarios were simulated. Two of these scenarios involved experimental personnel leaving the study area. In order to numerically model the effects of one or more persons moving through the study area and exiting the office, a first-order Immersed Boundary Method (IBM) was implemented in the CFD flow solver STREAM. Overall, CFD is able to generate very realistic flow and concentration fields in the indoor environment, even with the HVAC system turned off at an early stage in the experiment and with people moving through the study area. The detailed simulations permitted the following conclusions to be drawn and recommendations to be made.

For the SF₆ experiment, we believed that the flow rate measurements for the supply and return ducts are accurate. Therefore, it is hypothesized that the discrepancy between the numerical predictions and experimental measurements of concentration were mainly caused by (1) air flow leakage from cracks and crevices in the building envelope and, (2) dispersion of SF₆ in the HVAC system. Both these effects have not been accounted for in the current simulations. To address the first cause for the discrepancy, a 'blower door' experiment can be used to determine the locations of the leaks and the air flow rates through these leaks in the building shell. Alternatively, a series of new experiments can be conducted in an office

environment that has been certified to be airtight. To address the second cause for the discrepancy, the CFD model used here for the simulation of flow and dispersion in an open office can be coupled with a zonal model (such as COMIS or CONTAM), to simulate the flow and dispersion in the HVAC system. This CFD/zonal-model coupling should improve the numerical predictions for the SF₆ experiment and Scenario 0 (Baseline Case) for the BG release experiment, in which the HVAC system was turned on throughout the entire experiment.

The flow rate measurements for the supply and return ducts obtained for the SF₆ experiments were used in our simulations of the BG spore experiments. This is questionable for Scenarios 1 and 2, in which personnel are moving in the study area and the doors in Area I were closed. In both scenarios, unsteady CFD simulations were performed. Since both front and rear doors in Area I were closed as the various personnel exited the study area, the ventilation measurements in Area I alone will need to be modified as suggested by Eq. (3), the latter of which is based on the argument of global mass conservation in Area I. In theory, *time-dependent* flow rate measurements for the supply and return ducts should be made available and used as boundary conditions to perform the CFD simulations. As a minimum requirement to simulate the BG experiment, volumetric flow rates for the supply and return ducts should be measured for the following scenarios: (a) with only the two middle doors in Area I closed, and (b) with all four doors in Area I closed. To address the effects of BG spore deposition on the predictions, it is recommended that the present unsteady RANS approach be combined with an eddy interaction model (EIM, or random walk model) for modeling aerosol dispersion and deposition. EIM is based on a Lagrangian stochastic approach, in which individual particles are allowed to interact successively with discrete eddies (see, e.g., [21, 22]).

Finally, it should be emphasized here that the advantages of utilization of CFD modeling for assessment and design of mitigation strategies and protocols for defence against anthrax-tainted letters are obvious: (1) substantial reduction of lead times and costs of new designs involving other office configurations; (2) ability to study scenarios where controlled experiments are difficult or impossible to perform; and, (3) practically unlimited level of detail of results such as the flow field in the indoor environment and the concentration field of the dispersing BG spores (or, other contaminants) that are released into this flow field.

References

1. de Armond, P. (2002). The anthrax letters. Albion Monitor, <http://www.monitor.net/monitor/0208a/anthrax.html>.
2. Kournikakis, B.; Armour, S.J.; Boulet, C.A.; Spence, M.; and Parsons, B. (2001). Risk assessment of anthrax threat letters. *Defence Research Establishment Suffield*, DRES TR-2001-048.
3. Duncan, S.; Kournikakis, B.; and Ho, J. (2009). Pulmonary deposition of aerosolized *Bacillus atrophaeus* (BG) in an awake, unrestrained swine model due to exposure from a simulated anthrax letter incident. *Inhalation Toxicology*, 21(2), 141–152.
4. Kournikakis, B.; Walker, M.; Ho, J.; and Duncan, S. (2009). Statistical analysis of bacterial spore aerosols created by opening a spore containing “Anthrax Letter” in an office. *Journal of Aerosol Science*, 40(6), 514–522.

5. Kournikakis, B.; Ho, J.; and Duncan, S. (2010). Anthrax letters: personal exposure, building contamination and effectiveness of immediate mitigation measures. *Journal of Occupational and Environmental Hygiene*, 7(2), 71-79.
6. Price, P.N.; Sohn, M.D.; Lacomme, K.S.H.; and McWilliams, J.A. (2009). Framework for evaluating anthrax risk in buildings. *Environmental Science and Technology*, 43(6), 1783-1787.
7. Reshetin, V.P.; and Regens, D. (2004). Evaluation of malignant anthrax spore dispersion in high-rise buildings. *Journal of Engineering Physics and Thermophysics*, 77(6), 1155-1166.
8. Lien, F.S.; and Leschziner, M.A. (1994). A general non-orthogonal collocated finite volume algorithm for turbulent flow at all speeds incorporating second-moment closure, Part 1: Computational implementation. *Computer Methods in Applied Mechanics and Engineering*, 114 (1-2), 123-148.
9. Lien, F.S.; and Leschziner, M.A. (1994). Upstream monotonic interpolation for scalar transport with application in complex turbulent flows. *International Journal for Numerical Methods in Fluids*, 19(6), 527-548.
10. Leonard, B.P. (1979). A stable and accurate convection modelling procedure based on quadratic upstream interpolation. *Computer Methods in Applied Mechanics and Engineering*, 19(1), 59-98.
11. Patankar, S.V. (1980). *Numerical heat transfer and fluid flow*. Hemisphere Publishing Corporation.
12. Stone, H.L. (1968). Iterative solution of implicit approximations of multidimensional partial differential equations. *SIAM Journal on Numerical Analysis*, 5(3), 530-558.
13. Rhie, C.M.; and Chow, W.L. (1983). A numerical study of the turbulent flow past an isolated airfoil with trailing edge separation. *AIAA Journal*, 21(11), 1525-1532.
14. Aftosmis, M.J.; Berger, M.J.; and Melton, J.E. (1998). Robust and efficient cartesian mesh generation for component based geometry. *AIAA Journal*, 36(6), 952-960.
15. Peskin, C.S. (1977). Numerical analysis of blood flow in the heart, *Journal of Computational Physics*, 25(3), 220-252.
16. Tseng, Y.H.; and Ferziger, J.H. (2003). A ghost-cell immersed boundary method for flow in complex geometry. *Journal of Computational Physics*, 192(2), 593-623.
17. McCleery, R.E. (2006), National institute for occupational safety and health (NIOSH), *private communication*.
18. COMIS. <http://epb.lbl.gov/comis/>.
19. CONTAM. <http://www.bfrl.nist.gov/IAQanalysis/index.htm>.
20. Hsieh, K.J.; Lien F.S.; and Yee, E. (2007). Numerical modelling of scalar dispersion in an urban canopy. *Journal of Wind Engineering & Industrial Aerodynamics*, 95(12), 1611-1636.
21. Graham, D.I.; and James, P.W. (1996). Turbulent dispersion of particles using eddy interaction models. *International Journal of Multiphase Flow*, 22(1), 157-175.
22. Wang, L.P.; and Stock, D.E. (1992). Stochastic trajectory models for turbulent diffusion: Monte Carlo process versus Markov chains, *Atmospheric Environment, Part A*, 26 (9), 1599-1607.